Supporting Information

Bipolar Nano Impact Transients: Controlling the Redox Potential of Nanoparticles in Solution

Jonathan Markham[a], Neil P. Young[b], Christopher Batchelor-McAuley[a] and Richard G. Compton[a]*

(a) University of Oxford, Department of Chemistry, Physical and Theoretical Chemistry Laboratory, Oxford University, South Parks Road, Oxford, OX1 3QZ (UK)

(b) University of Oxford, Department of Materials, Parks Road, Oxford OX1 3PH (UK)

Corresponding Author

*Richard G. Compton, E-mail: Richard.compton@chem.ox.ac.uk

Contents

Section 1; Transmission Electron Microscopy Characterisation

The nanoparticles used in this work have been extensively characterised using transmission electron microscopy (TEM) both in the main text and in previous work[1-4]. Samples were prepared for imaging by removing the citrate capping from the porous nanoparticles by washing with NaOH[5], then exposing to an aqueous solution containing molecular iodine at a concentration of 0.025 mM for one hour. Nitrogen gas was then bubbled through the resulting

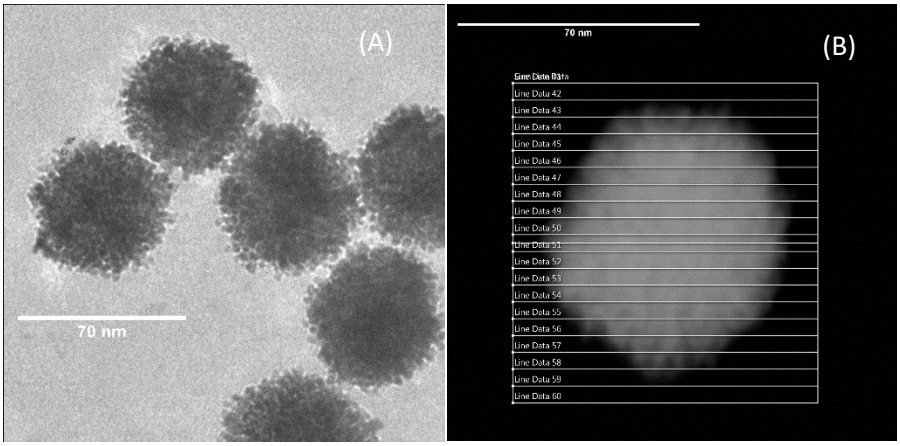

Figure S1: (A) HR-CTEM image of the mesoporous 70 nm dimeter Pt nanoparticles. (B) HAADF STEM image of representative 70 nm Pt nanoparticle, solid lines represent individual lines along which electron beam scanned to create sum spectrum.

solution causing excess iodine to volatise and be removed. Finally 6 µL of the nanoparticle suspension was deposited onto a 400 mesh gold grid coated with holey carbon. The grids were stored under vacuum prior to imaging to reduce contamination. The platinum nanoparticles used were citrate capped mesoporous in an aqueous 4 mM citrate solution, and had a nominal diameter of 70 nm (69.2 ± 4.2 nm). The nanoparticles themselves are made up of smaller crystallites which had diameters in the range 3.37 – 6.08 nm.

Figure S1 (A) is a high resolution conventional TEM image of the 70 nm PtNPS recorded on a JEOL 3000F FEGTEM with an accelerating voltage of 200 keV. It shows the crystallites which

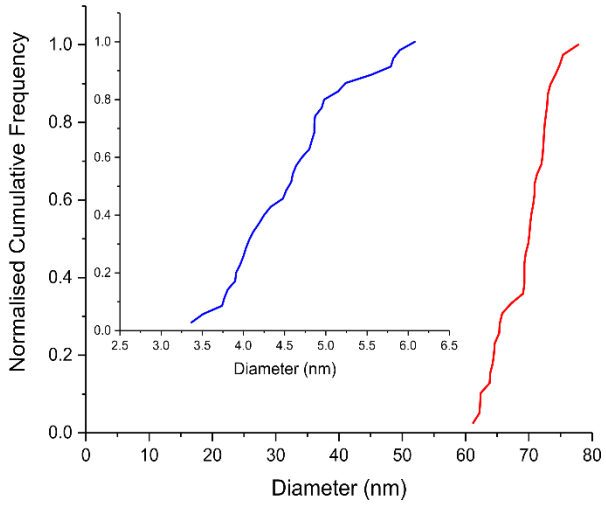

Figure S2: Size distribution plots of normalised cumulative frequency against particle diameter for both the 70 nm nanoparticles (red), and the individual crystallites which make up the nanoparticles (blue)

make up the overall mesoporous nanoparticle structure. These images were used to evidence the overall mesoporous structure of the nanoparticles and to provide size distributions both for the nanoparticles themselves, and for the individual crystallites (figure S2 red and blue respectively). The nanoparticle sizes were determined using ImageJ software from the National Institutes of Health and the Laboratory for Optical and Computational Instrumentation to measure 2D projected area, and this was converted into an effective diameter. Figure S1 (B) is a high angle annular dark field STEM image of a representative nanoparticle. The image shows the individual lines along which the electron beam scanned to create the sum spectrum for the overall particle. The image scanned had a resolution of 1024 pixels and a dwell time of 10 µs was used. This resulted in a pass live time of 3 s, and there were 10 total passes for each individual line.

The expected iodine to platinum ratio for a perfectly solid spherical particle was calculated using the following equation

$$\left(\frac{4\pi r^2 \sigma f}{F}\right) \Big/ \left(\frac{\frac{4}{3}\pi r^3 \rho_{Pt}}{Ar_{Pt}}\right) \times 100 \qquad (1)$$

where σ is the specific charge density for H_{upd} (210 μC cm^{-2}), f is the fractional surface coverage (0.40), F is the Faraday constant (96485 C mol^{-1}), ρ_{Pt} is the density of platinum (21.45 g cm^{-3}) and Ar_{Pt} is the molar mass of platinum (195 g mol^{-1}).

Section 2: Underpotential Deposition of Hydrogen

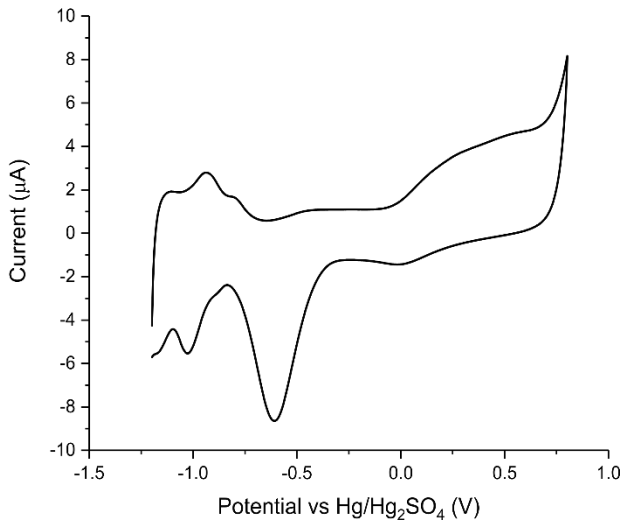

Figure S3: Voltammetric response of Pt macro-electrode in 20 mM KNO_3 after repeated cycles (10 cycles) up to 0.8 V at a scan rate of 100 mV/s scanned anodically from -1.2 V

Figure S3 shows the voltammetric response of a platinum macro-electrode in 20 mM KNO_3 after 10 scans from -1.2 -- +0.8 V (vs Hg/Hg_2SO_4). The location of the hydrogen underpotential deposition (H_{upd}) peaks in a voltammetric scan are sensitive to the pH local to the electrode. In 20 mM KNO_3 there is a low buffering capacity, as the pH is controlled by the presence of dissolved carbon dioxide, causing the H_{upd} region to become distorted (see red line Fig. 2 main text). However, if successive scans are undertaken up to +0.8 V, the H_{upd} region becomes well defined and at a more negative potential. This is due to the formation and subsequent reduction of platinum oxide on the anodic scan, which causes a local increase in pH at the electrode surface temporarily leading to a defined H_{upd} response at a potential consistent with an alkaline environment.

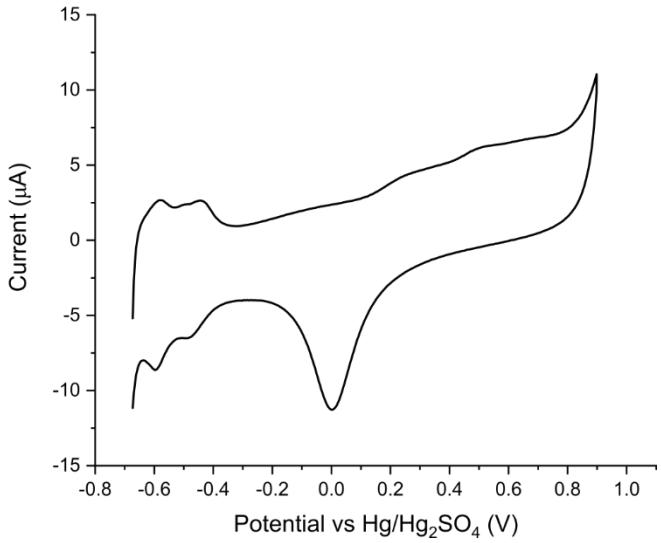

Figure S4: Voltammetric response of glassy-carbon macro-electrode modified by drop-casting 5 μL of 70 nm platinum nanoparticles in 0.1M H_2SO_4 after repeated cycles (10 cycles) up to 0.9 V at a scan rate of 100 mV/s scanned anodically from - 0.675 V

Figure S4 shows the voltammetric response of a glassy carbon electrode of diameter 2.94 mm modified by drop-casting 5 μL of 70nm of platinum nanoparticles in 0.1M H_2SO_4 after 10 scans from -0.675 -- +0.9 V (vs Hg/Hg_2SO_4). The H_{upd} peaks in this scan are more distorted than is the case for the same system but using a polycrystalline Pt electrode. This is due to the background contribution due to the capacitive charging of the glassy-carbon electrode.

Section 3: Iodine Adsorption on polycrystalline platinum

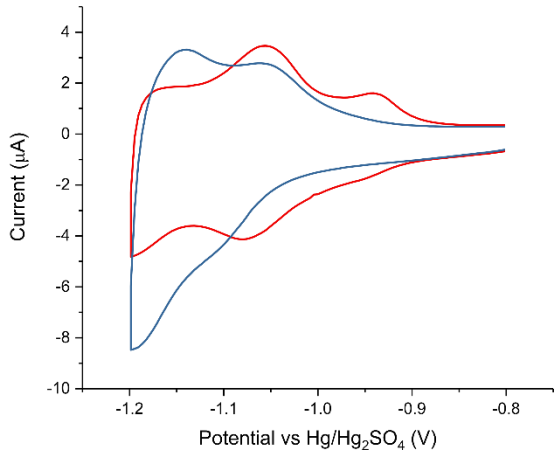

Figure S5: Voltammetric response of Pt macro-electrode around the H_{upd} region in 20 mM KOH at 100 mV/s for both a clean electrode (red) and one which has been exposed to an aqueous solution containing 0.1 mM molecular iodine for 1 minute (blue)

Figure S5 shows the voltammetric response of a platinum macro-electrode in 20 mM KOH in both the absence of iodine (red) and having been exposed to a 0.1 mM solution of iodine. The presence of iodine adsorbed on platinum is most clearly evidenced electrochemically through indirect methods, such as inhibition of H_{upd} processes, which can clearly be seen in acid conditions. However, in this case in alkaline conditions, the H_{upd} process is only partially blocked as shown in figure S5 above, which shows the voltammetric response of a clean electrode and one exposed to an aqueous solution containing molecular iodine in 20 mM KOH.

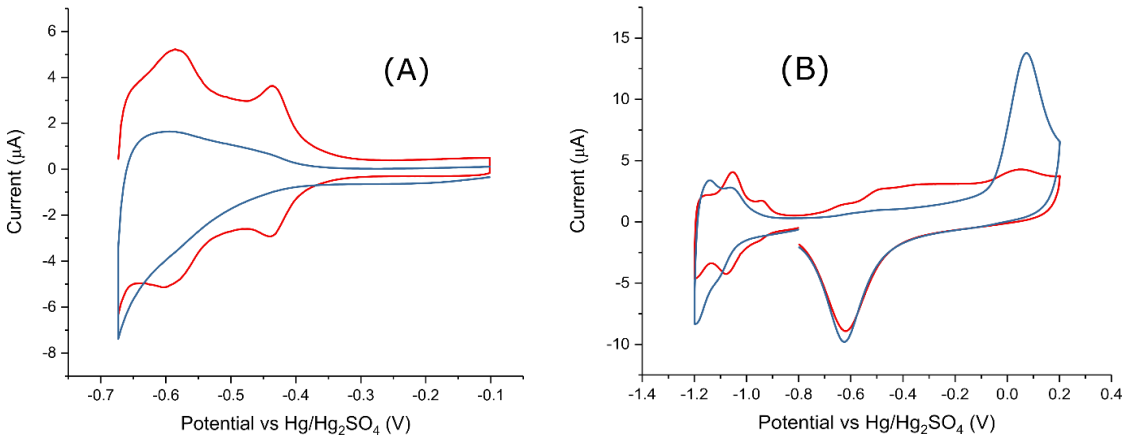

Figure S6: Voltammetric evidence that iodine is still present on the Pt surface in alkaline conditions. (A) presents the voltammetric response of Pt macro-electrode in 0.1 M H_2SO_4 for both clean electrode (red) and electrode exposed to an aqueous solution containing 0.1 mM molecular iodine (blue) after first scanning twice around the H_{upd} region in 20 mM KOH then transferring to the acid conditions. (B) presents the voltammetric response in 20 mM KOH for the two conditions: the clean electrode (red) and the electrode exposed to an aqueous solution containing 0.1 mM molecular iodine for 1 minute, both scanned up to +0.2 V

The iodine, however, is still present on the Pt surface, and can be evidenced in figure S6. First, (A) is the voltammetric response of the H_{upd} region for the transfer of the iodine covered electrode to an acid solution (0.1 M H_2SO_4) after being in an alkaline solution (20 mM KOH), where in this alkaline solution the electrode was voltammetrically scanned showing a voltammetric response akin to that reported in the Figure S5. Upon transfer of this electrode to the acidic conditions the voltammogram shows the characteristic inhibition response as would be expected for adsorbed iodine. Second, (B) is the voltammetric response of the clean and iodine covered electrodes in 20 mM KOH scanned over the potential range of -1.2 -- +0.2 V (vs Hg/Hg_2SO_4). This shows inhibition of the onset of platinum oxidation from -0.8 V for the clean electrode to -0.55 V for the iodine modified electrode. This is consistent with iodine being present on the Pt surface.

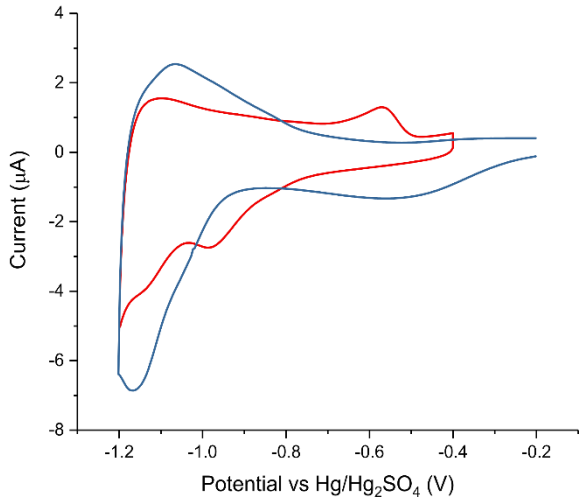

Figure S7: Voltammetric response of Pt macro-electrode around the H_{upd} region in 20 mM KNO_3 at 100 mV/s for both a clean electrode (red) and one which has been exposed to an aqueous solution containing 0.1 mM molecular iodine for 1 minute (blue)

Similarly, if the same system as described above is investigated using non-buffered 20 mM KNO_3 as the electrolyte instead of 20 mM KOH there is only a minimal change in the H_{upd} response in the presence of iodine. This is shown in figure S7, which presents the voltammetric response in non-buffered conditions in the presence and absence of iodine (red and blue respectively). Here the minimal change in the response is the inhibition of the onset of the H_{upd} on the cathodic scan, and the distortion of the H_{upd} peaks on the anodic scan. Again, comparatively to the alkaline case, the iodine can be evidenced to be adsorbed on the platinum by way of transfer to an acid solution and observing the clear blocking of the H_{upd}, or by inhibition of platinum oxide onset.

Iodine which is adsorbed on a platinum surface can, however be evidenced to be removed by exposure to a solution saturated with hydrogen, as shown in figure S8. Here the response of a platinum macro-electrode in a 2 0mM KNO_3 + 1 mM HNO_3 electrolyte in the H_{upd} region was investigated. The red line shows the response in the absence of iodine, the blue line shows the

response of the electrode after exposure to a 0.1 mM solution of iodine for 1 minute, then an aqueous solution saturated with hydrogen (0.78 mM) for 5 minutes. The yellow line shows the response of the electrode after exposure to a 0.1 mM solution of iodine for 1 minute, then an aqueous solution for 5 minutes.

The voltammetric response returned is comparable to that of the clean electrode. This can be ascribed to the hydrogen removing the adsorbed iodine from the Pt surface.

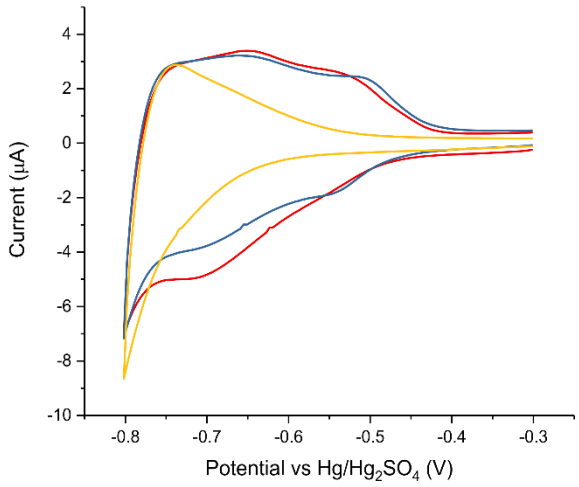

Figure S8: Voltammetric response of Pt macro-electrode around the H_{upd} region in 20 mM KNO_3 + 1 mM HNO_3 electrolyte. Red shows the response for a clean electrode. Blue is the response for an electrode which has been exposed to an aqueous solution containing 0.1 mM molecular iodine for 1 minute, then a saturated hydrogen solution (0.78 mM) for 5 minutes. Yellow is the response for an electrode exposed to the same iodine solution for 1 minute, then deionised water for 5 minutes.

Section 4: Platinum H_{upd}: nano-impacts

The oxidative and reductive spike charges measured on a gold micro-electrode in a solutions of 20 mM KNO_3 and 3.0 pM platinum nanoparticles under hydrogen and nitrogen respectively which we have so far associated with the H_{upd} are found to differ in magnitude by up to ~25 % depending on the measurement conditions, as shown in table S1 (see main text for full experimental conditions). It is insightful to consider the possible origin of this discrepancy.

Potential (V)	-1.2	-0.1	0	+0.25
N_2	0.30 ± 0.006	No features	No features	No features
$N_2 + I_2$	0.33 ± 0.006	No features	No features	No features
H_2	No features	0.26 ± 0.012	0.26 ± 0.017	0.30 ± 0.029[1]
$H_2 + I_2$	0.26 ± 0.013	No features	No features	No features

Table S1: Spike charges (pC) measured in a solution containing 20 mM KNO_3 and 3 pM PtNPs degassed with either nitrogen or hydrogen. For iodine containing solutions, the nanoparticle solution as provided was pre-mixed with excess solid iodine for 10 minutes before addition of the potassium nitrate solution and degassing.

First, in the main text we assumed that the current spikes are under these conditions solely related to the deposition or removal of hydrogen from the nanoparticle surface. However, capacitive charging of the nanoparticle will also contribute to the charge passed. The experimental values measured and presented in table S1 above are a combination of Faradic plus capacitive charge. For a metallic surface the specific capacitance is commonly of the order to 20 μF cm^{-2}. Hence, if the nanoparticle changes in potential by 1 volt this corresponds to the passing of 20 μC cm^{-2}. In comparison the specific charge density for H_{upd} is approximately 210 μC cm^{-2}. Hence, if the nanoparticle changes potential by 1 V then approximately 10 % of the current will be associated not with the Faradaic H_{upd} process but with the capacitive charging of the nano-platinum interface. As evidenced in the main body of the text the solution phase potential of the nanoparticles depends on its chemical environment; consequently, it is plausible that some of the

measured discrepancy may be explained in terms of variable capacitive charging of the nano material.

Second, the shape and hence duration of the oxidative spike varies depending on the experimental system. As shown in Figure S9, the oxidative spikes measured at -0.1 and 0.0 V exhibit long current tails. The different conditions which result in the switching from oxidative to reductive spikes also result in different shapes for those spikes, and those spikes with long current tails will include charge from the nano-event within the tail. Hence this current tail must be included in any integrative analysis of the spikes themselves, which could plausibly result in missed charge for the nano-event from that within the tail. This issue with the long duration of the oxidative nano-impact events likely explains why the measured oxidative charge is smaller than that reported from the reduction process. Ultimately, the measured charge is sensitive to the system's signal to noise ratio, if a spike is long in duration or if the system's noise is larger, then this will lead to the spike's charge to be likely under estimated. Hence, the actual charge associated with a nano-event can be larger than measured due to the limitations of the system's signal-to-noise ratio. This bias towards under estimating the magnitude of the nano-impact event is not reflected in the measured error bars.

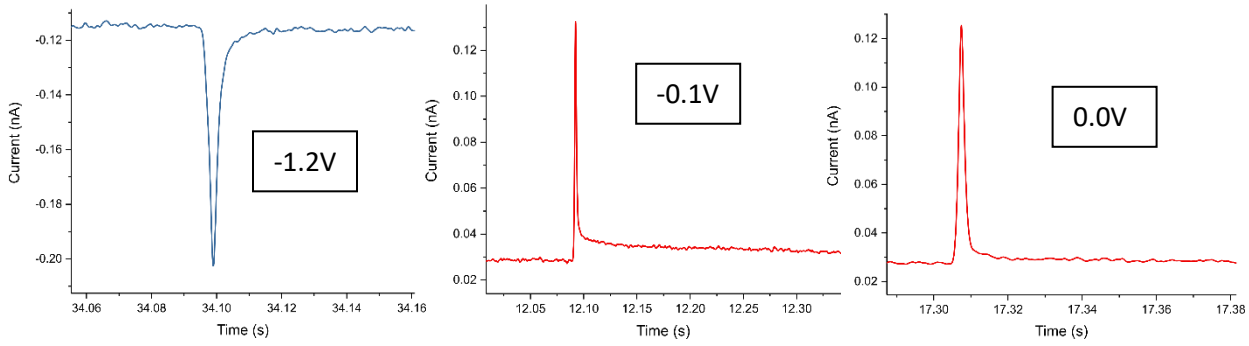

Figure S9: Representative spike features observed at -1.2, -0.1 and 0.0 V (left, middle and right respectively) in a solution of 20 mM KNO_3 with 3 pM 70 nm PtNPs saturated with nitrogen (for -1.2 V) or hydrogen (for -0.1 and 0.0 V); $[H_2]$ = 0.78 mM.

Section 5: Voltammetric response of Au microelectrode in an iodine solution

Solution phase iodine can be electrochemically reduced by a gold electrode, with a standard redox couple for iodine/iodide of -0.100 V (vs Hg/Hg_2SO_4). The iodine reduction is evidenced

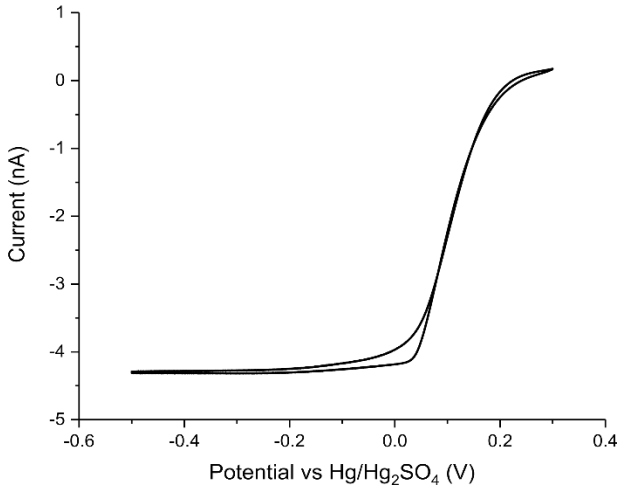

Figure S10: Voltammetric response of Au microelectrode in 0.1 mM iodine solution at a scan rate of 100 mV/s

below in figure S10, which shows the voltammetric response of an Au microelectrode of radius 2.5 µm in a solution of 0.1 mM iodine. The iodine reduction can be seen to occur at potentials below +0.1 V and reaches a steady state current of -4.28 nA. This reduction potential is shifted to slightly more positive than its standard state redox potential due to the lack of iodide in the bulk solution.

The expected half-wave potential for this reduction may also be calculated using the following equation[6].

$$\exp\left(n\theta_{\frac{1}{2}}\right) = c^{\ominus(q-m)} c_A^{*(m-q)} 2^{(q-m)} \left(\frac{m\delta_A D_B}{q\delta_B D_A}\right)^q \qquad (2)$$

where $\theta_{1/2}$ is the dimensionless half-wave potential, $c^{\ominus}$ is the standard potential (1 mol dm^{-3}), c^*_A is the concentration of species A in the bulk solution (mol dm^{-3}), δ_A is the diffusion layer

thickness of species A (m), D_A is the diffusion coefficient of A (m^2 s^{-1}), and m, n, and q are stoichiometric coefficients in the electrochemical reduction of species A to B:

$$mA + ne^- \rightleftharpoons qB \quad (3)$$

Using this method, a value of 0.106 V is returned, which is in close agreement to the value of 0.109 V extracted from the figure above.

1. Yu, W.; Batchelor-McAuley, C.; Chang, X.; Young, N. P.; Compton, R. G., Porosity Controls the Catalytic Activity of Platinum Nanoparticles. *Physical Chemistry Chemical Physics* **2019**, *21*, 20415-20421.
2. Jiao, X.; Batchelor-McAuley, C.; Lin, C.; Katelhon, E.; Tanner, E. E. L.; Young, N. P.; Compton, R. G., Role of Nanomorphology and Interfacial Structure of Platinum Nanoparticles in Catalyzing the Hydrogen Oxidation Reaction. *Acs Catalysis* **2018**, *8*, 6192-6202.
3. Jiao, X.; Lin, C.; Young, N. P.; Batchelor-McAuley, C.; Compton, R. G., Hydrogen Oxidation Reaction on Platinum Nanoparticles: Understanding the Kinetics of Electrocatalytic Reactions Via "Nano-Impacts". *The Journal of Physical Chemistry C* **2016**, *120*, 13148-13158.
4. Yu, W.; Batchelor-McAuley, C.; Wang, Y.-C.; Shao, S.; Fairclough, S. M.; Haigh, S. J.; Young, N. P.; Compton, R. G., Characterising Porosity in Platinum Nanoparticles. *Nanoscale* **2019**, *11*, 17791-17799.
5. Moglianetti, M.; Solla-Gullón, J.; Donati, P.; Pedone, D.; Debellis, D.; Sibillano, T.; Brescia, R.; Giannini, C.; Montiel, V.; Feliu, J. M., Citrate-Coated, Size-Tunable Octahedral Platinum Nanocrystals: A Novel Route for Advanced Electrocatalysts. *ACS applied materials & interfaces* **2018**, *10*, 41608-41617.
6. Jiao, X.; Batchelor-McAuley, C.; Kätelhön, E.; Ellison, J.; Tschulik, K.; Compton, R. G., The Subtleties of the Reversible Hydrogen Evolution Reaction Arising from the Nonunity Stoichiometry. *The Journal of Physical Chemistry C* **2015**, *119*, 9402-9410.